



# Migratory strategy drives species-level variation in bird sensitivity to vegetation green-up

Casey Youngflesh<sup>1</sup>, Jacob Socolar<sup>2,3</sup>, Bruna R. Amaral<sup>4</sup>, Ali Arab<sup>5</sup>, Robert P. Guralnick<sup>6</sup>, Allen H. Hurlbert<sup>7,8</sup>, Raphael LaFrance<sup>6</sup>, Stephen J. Mayor<sup>9</sup>, David A. W. Miller<sup>4</sup> and Morgan W. Tingley<sup>1,2</sup>✉

**Animals and plants are shifting the timing of key life events in response to climate change, yet despite recent documentation of escalating phenological change, scientists lack a full understanding of how and why phenological responses vary across space and among species. Here, we used over 7 million community-contributed bird observations to derive species-specific, spatially explicit estimates of annual spring migration phenology for 56 bird species across eastern North America. We show that changes in the spring arrival of migratory birds are coarsely synchronized with fluctuations in vegetation green-up and that the sensitivity of birds to plant phenology varied extensively. Bird arrival responded more synchronously with vegetation green-up at higher latitudes, where phenological shifts over time are also greater. Critically, species' migratory traits explained variation in sensitivity to green-up, with species that migrate more slowly, arrive earlier and overwinter further north showing greater responsiveness to earlier springs. Identifying how and why species vary in their ability to shift phenological events is fundamental to predicting species' vulnerability to climate change. Such variation in sensitivity across taxa, with long-distance neotropical migrants exhibiting reduced synchrony, may help to explain substantial declines in these species over the last several decades.**

Phenology, that is the timing of seasonal life history events such as migration and reproduction, has changed substantially in response to ongoing global change across a wide variety of taxa and in all the Earth's biomes<sup>1,2</sup>. There is increasing concern that variation in the magnitude and direction of these changes is resulting in altered species interactions<sup>3,4</sup> both among (via phenological mismatch<sup>5,6</sup>) and within (via competition<sup>7</sup>) trophic levels. This may ultimately have implications for ecosystem function, by way of population<sup>8</sup> and coexistence dynamics<sup>9</sup>. However, despite the growing documentation of widespread phenological change, much remains unknown regarding how and why these responses vary across space and among species<sup>2</sup>.

Given their reliance on seasonally available resources and their widespread monitoring by the public, migratory birds represent a valuable means to understand phenological change. These birds must time migration and breeding to take advantage of temporal fluctuations in resources and maximize fitness. As such, the arrival of migratory birds has been heralded as a harbinger of seasonal change dating back at least to ancient Greece<sup>10</sup>. Coincident with changes observed in other organisms<sup>1</sup>, many bird species are now migrating substantially earlier in spring than they did just decades before<sup>8,11–13</sup>. In North America, many of these migratory species, particularly neotropical migrants, have experienced dramatic population losses over the past half-century<sup>14</sup>. Understanding how phenological dynamics vary among species, particularly in response to spatiotemporal fluctuations of lower trophic levels<sup>3</sup>, is a key step in characterizing and predicting the consequences of phenological

asynchronies, including the role that these might play in observed long-term populations declines.

Quantifying variation in migration phenology across species, space and time requires vast quantities of biological survey data that are only now becoming available via resources such as large-scale community-science databases. For over 7 million bird observations submitted to the program eBird<sup>15</sup>, we used logistic generalized additive models (GAMs) to derive estimates of migratory arrival dates for 56 species of birds from 2002 to 2017 across 33° of latitude in eastern North America (Extended Data Figs. 1 and 2). We used these estimates in conjunction with hierarchical Bayesian spatial autoregressive models to derive annual estimates of migration phenology for each species (Extended Data Figs. 3 and 4). With these estimates, we quantified the 'sensitivity' of birds to spring phenology, defined by how well the timing of spring migration of birds tracks interannual fluctuations in vegetation phenology and addressed how and why sensitivity varied across space and among species.

## Results and discussion

**Variation in sensitivity across space.** Green-up (the timing of the vernal emergence of new vegetation)<sup>16</sup> is a key indicator of the arrival of spring<sup>17</sup>, linked to the availability of key food resources for migratory birds<sup>18</sup>. As such, it represents a principal metric against which to evaluate phenological change, particularly in the absence of direct information on food availability<sup>19</sup> (which is sparse in the case of North American migratory birds). We found that, while spring bird arrival does broadly coincide with interannual

<sup>1</sup>Department of Ecology and Evolutionary Biology, University of California, Los Angeles, CA, USA. <sup>2</sup>Department of Ecology and Evolutionary Biology, University of Connecticut, Storrs, CT, USA. <sup>3</sup>Faculty of Environment and Natural Resources Management, Norwegian University of Life Sciences, Ås, Norway. <sup>4</sup>Department of Ecosystem Science and Management, Pennsylvania State University, University Park, PA, USA. <sup>5</sup>Department of Mathematics and Statistics, Georgetown University, Washington, DC, USA. <sup>6</sup>Florida Museum of Natural History, University of Florida, Gainesville, FL, USA. <sup>7</sup>Department of Biology, University of North Carolina, Chapel Hill, NC, USA. <sup>8</sup>Environment, Ecology and Energy Program, University of North Carolina, Chapel Hill, NC, USA. <sup>9</sup>Ontario Forest Research Institute, Ontario Ministry of Natural Resources and Forestry, Sault Ste. Marie, Ontario, Canada. ✉e-mail: [mtingley@ucla.edu](mailto:mtingley@ucla.edu)

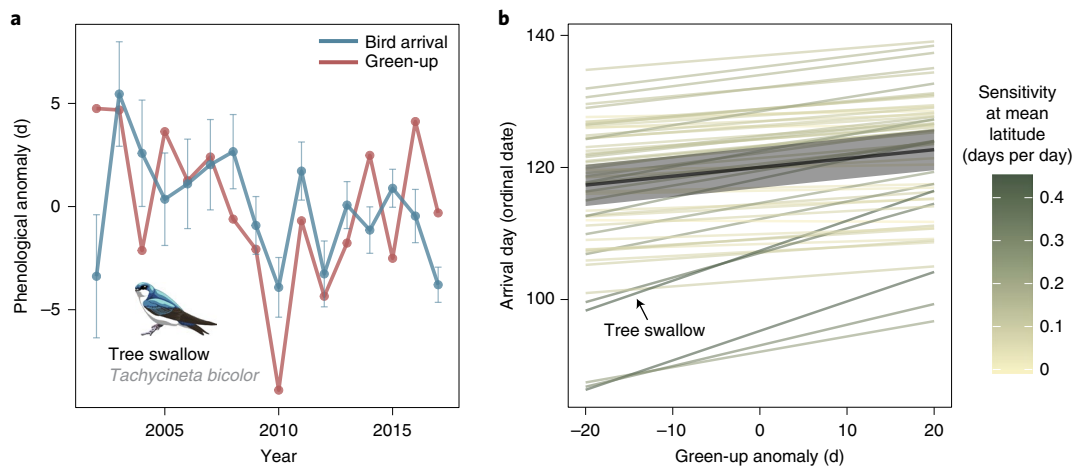


**Fig. 1 | Bird arrival in response to green-up.** **a**, Interannual variation in green-up (red) and arrival dates for a representative species, the tree swallow (blue; both variables centred), for a single, representative location (cell centroid: 43.78° N, 75.00° W) in the species' range. Error bars for arrival represent 1 posterior s.d. **b**, When analysed across the entire breeding and migratory ranges of 56 species, spring arrival dates (plotted at each species' mean latitude) showed variable sensitivity to green-up anomalies (that is, centred on the mean green-up value for each cell). Each line represents one bird species. Colours represent the slope of the lines—the extent to which arrival date changes given a 1-d change in green-up—which corresponds to sensitivity. Dark green hues denote higher sensitivity while yellow hues denote lower sensitivity. The black line represents the overall (cross-species) mean relationship between arrival and green-up anomaly, while the grey ribbon denotes the 95% credible interval. For enhanced visualization and exploration of single-species trends, see <https://migratory-sensitivity.shinyapps.io/MigSen-app/>.

fluctuations in forest green-up (as measured by satellite-based sensors), birds only coarsely track these changes in vegetation phenology (Fig. 1). For every 1-d change in green-up, local bird arrival phenology ( $\alpha_i$  in equation (12)) changed by only 0.13 d (95% CI 0.11, 0.16; Figs. 1 and 2 and Extended Data Fig. 5) across all species. We refer to this relationship of the number of days change in bird arrival per day change in green-up as 'sensitivity'—of which a value of 1 represents a scenario where these metrics fluctuate perfectly in synchrony. In all cases, sensitivity was calculated relative to the annual anomalies in green-up for a given location. Green-up also exhibited higher interannual variation (s.d. = 5.31 d) compared to variation in bird arrival (across species mean s.d. = 1.70 d; Fig. 1). These results suggest that migratory birds may have a limited capacity to maintain synchrony with changes in phenology at lower trophic levels (whether that be interannual fluctuations or long-term changes). Given that green-up is advancing over time (Extended Data Fig. 6), our results are consistent with a previous finding that asynchrony between birds and vegetation is increasing over time<sup>12</sup>.

On average, green-up explained ~19% of the variation (equation (15)) in arrival (with species-level means ranging from 2 to 66%) within geographic regions (defined by hexagonal cells of ~70,000 km<sup>2</sup>; Extended Data Fig. 1). While the seasonal nature of resource availability is thought to be the primary reason why migration evolved as a viable strategy<sup>20</sup>, migratory birds face challenges in timing life history events to match year-to-year variation in these resource pulses<sup>21</sup>. During the overwinter period, birds have limited information about conditions on breeding grounds. Migrants may rely on cues such as photoperiod<sup>22</sup> or other abiotic<sup>23</sup> or biotic<sup>24,25</sup> conditions to time their departure from overwintering grounds. Given the limited covariation between conditions at overwintering and breeding grounds, these cues provide only a coarse approximation of when birds must depart to synchronize their arrival with temporal variation in resource availability, limiting how well migratory birds can track spring phenology.

Within species, we observe a strong latitudinal gradient in sensitivity to green-up ( $\mu_{\gamma_{APG}}$  (equation (13)) posterior mean: 0.009 unit (days arrival per day green-up) change in sensitivity per degree latitude, 95% CI 0.006, 0.012), with birds generally less sensitive to

fluctuations in green-up in the southern portions of their migratory and breeding range compared to the northern portions (Fig. 2 and Extended Data Fig. 5; this pattern is also apparent when considering only the breeding range, Supplementary Information). This latitudinal gradient in sensitivity, in conjunction with faster phenological change in vegetation at higher latitudes (Extended Data Fig. 6), may explain why phenological change is generally more pronounced at higher latitudes for birds and other vagile taxa<sup>13,26</sup>. This finding also suggests that most birds have some capacity to adjust their migratory behaviour en route on the basis of environmental conditions<sup>25</sup> (in effect, riding the 'green wave' of vegetation across space and time<sup>27</sup>) but that increases in migration speed can only be achieved incrementally (probably through adjustments in stopover duration<sup>28</sup>). As a result, bird phenology generally more strongly matches fluctuations in green-up at higher latitudes (Fig. 2). Birds may also respond more strongly to green-up in the more polar portions of their ranges because these areas are more likely to reflect conditions on breeding grounds. We caution, however, that even the most sensitive species in the most responsive portions of their range still fail to keep pace with changes in green-up (Fig. 2 and Extended Data Fig. 5). Still, spatial trends in phenological sensitivity are consistent with other work that has shown that birds adjust their migratory speed in response to changes in temperature<sup>29,30</sup> and that bird arrival dates on the northern Gulf of Mexico coastline have changed little over time<sup>31</sup>.

Intraspecific variation may also play a role in this spatial variation in sensitivity. Populations within the same species may vary in their degree of plasticity to environmental conditions<sup>32</sup>, exhibit different migratory strategies (perhaps using different migratory corridors) or face different constraints resulting from conditions experienced on overwinter grounds. These intraspecific differences could explain departures from the general latitudinal pattern in sensitivity for some species, including reverse latitudinal trends and longitudinal patterning (Fig. 2). For example, the northern parula *Setophaga americana* shows higher sensitivity in the southeast portion of its North American range, possibly the result of spatially discrete overwintering populations (for example, on Caribbean islands and along the Yucatán Peninsula) that probably experience differing environmental conditions in migration along distinct corridors.

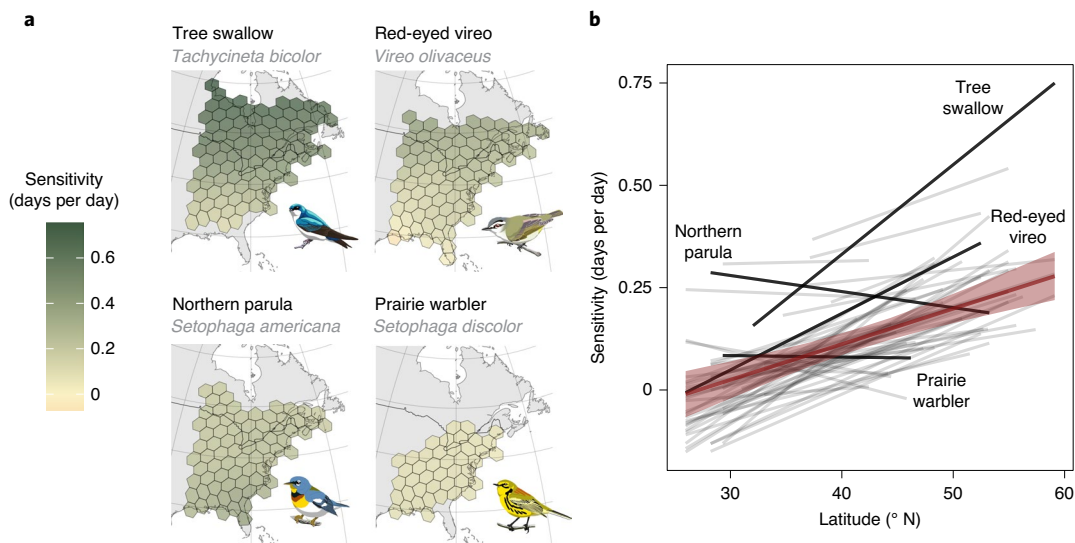


**Fig. 2 | Spatial variation in the sensitivity of bird arrival to green-up.** Sensitivity represents the magnitude of change in bird arrival per day change in green-up. **a**, Variation in arrival sensitivity over space for four representative bird species included in our study. Colours represent the cell-specific posterior mean estimates of sensitivity, with dark green hues denoting a stronger relationship between arrival and green-up and yellow hues denoting a weaker relationship. Cells are gridded over the portion of species' migratory and breeding ranges that fell within our study area. **b**, Arrival sensitivity to green-up as a function of latitude, showing a general pattern of increasing sensitivity with latitude. Black lines represent individual species, with bold lines corresponding to species presented in **a**. The red line represents the mean relationship across species between sensitivity and latitude, while the red ribbon denotes the 95% credible interval.

**Variation in sensitivity among species.** Among the 56 bird species we studied, species varied widely in their mean sensitivity to advancing green-up (Figs. 1 and 2 and Extended Data Fig. 5). We found that species that migrate more slowly, arrive earlier and overwinter further north are more sensitive to changes in green-up ( $\beta_{\xi}$  in equation (12)) posterior mean effect PC1  $-0.038$ , 95% CI  $-0.057$ ,  $-0.019$ ; Fig. 3; see also Supplemental Information for discussion of other migratory traits). For example, the pine warbler (*Setophaga pinus*) and eastern phoebe (*Sayornis phoebe*), which lie on one end of the spectrum (Supplementary Table 1), vary their arrival dates substantially in response to changes in green-up ( $\xi_{APG_k}$  in equation (11)—posterior means 0.37 (pine warbler) and 0.45 (eastern phoebe) days per day; Extended Data Fig. 5), whereas the bobolink (*Dolichonyx oryzivorus*) and willow flycatcher (*Empidonax traillii*), which lie on the other end of the spectrum (Supplementary Table 1), vary only a small amount ( $\xi_{APG_k}$ —posterior means 0.08 (bobolink) and 0.11 (willow flycatcher) days per day; Extended Data Fig. 5). Species that exhibit greater sensitivity also tend to have larger inter-annual variability in arrival dates ( $\rho$  in equation (18))—posterior mean 0.86, 95% CI 0.80, 0.90), suggesting that phenological inflexibility in migration is a primary driver of insensitivity to green-up.

The novel trait relationships illustrated in this work connect recent research on the natural history of avian migration to our understanding of mechanisms underlying phenological shifts. Migratory birds in eastern North America can be generally divided into neotropical migrants—that largely winter in the Caribbean or Central and South America—and temperate-wintering migrants—that remain predominantly in the United States and northern Mexico. Temperate-wintering migrants have northern range limits that vary dynamically in winter<sup>33</sup> and show strong relationships to thermal physiology<sup>34</sup>, leading to spring migrations that begin early, traverse relatively short distances and progress slowly<sup>35</sup>. In contrast, neotropical migrants have winter ranges that largely appear to track resource availability<sup>36</sup>, leading to longer migrations that arrive later but progress more quickly<sup>35</sup>. Previous synthetic efforts have come to mixed conclusions regarding the ability of short- versus

long-distance migrants to respond to phenological change<sup>37</sup>. Our findings suggest that these two groupings broadly characterize the continuous spectrum of migratory species' sensitivity of arrival to green-up in North America (Fig. 3). Temperate-wintering migrants benefit from better access to information about resource conditions at their migratory destinations so as to arrive earlier as needed yet dynamically avoid the hazards of early-spring weather. In contrast, neotropical migrants are limited by resource availability and weak teleconnections between wintering and breeding ranges, thus leading to later, faster and more inflexible migration.

**Implications for understanding global change.** Given that advances in spring green-up are likely to continue into the future<sup>38</sup>, our results suggest that particular species (those that overwinter closer to breeding grounds, migrate more slowly and arrive earlier) may be better equipped to keep pace with some components of future global change. Much of the concern over differential shifts in phenology across trophic levels is due to the risk of phenological mismatch<sup>6</sup>. Species that adjust their arrival dates to match changes in green-up may better match changes in the timing of resource availability, whereas less sensitive species may be at risk of phenological mismatch where breeding success or adult survival is depressed as a result of these temporal asynchronies<sup>39</sup>, with implications for population dynamics<sup>40</sup>. Evidence for the negative demographic consequences of phenological mismatches remains sparse<sup>41,42</sup>, however, highlighting the need to not only quantify apparent asynchronies but also to evaluate their consequences. Future efforts should integrate these findings into a tritrophic framework<sup>43</sup>, whereby insect dynamics<sup>44</sup>, particularly larval lepidopterans, and demographic responses are considered directly. The role of rapid evolution in shaping phenological responses should also not be discounted and may provide a means of adaptation to directional phenological change<sup>45</sup>.

Beyond trophic mismatches, species-level variation in arrival phenology may lead to an assortment of cascading effects on life history and demography. More sensitive species might also stay longer on breeding grounds, which could lead to population gains

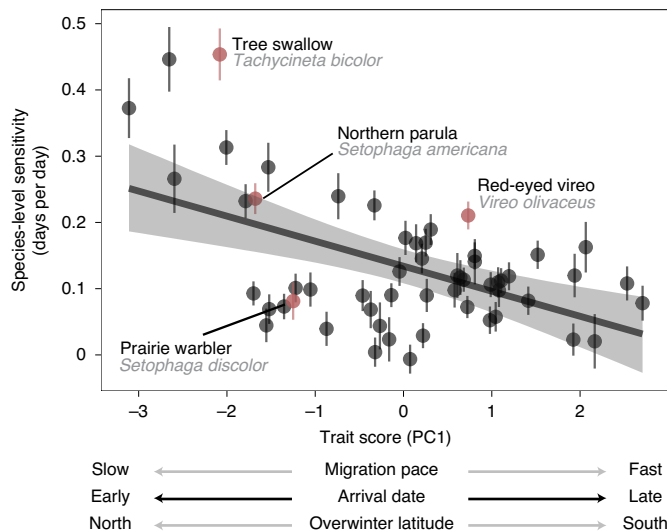


**Fig. 3 | Species-level sensitivity in the timing of bird arrival to fluctuations in green-up as a function of migratory traits.** Correlated migratory traits are combined into a single principal component axis, PC1, for which negative values are associated with slower migration pace, earlier arrival dates and more northerly overwinter latitudes. Each point represents one species. Error bars represent 1 posterior s.d. Red points highlight species presented in Fig. 2. The black line represents the mean relationship between species-level sensitivity and the migratory traits of interest, while the grey ribbon denotes the 95% credible interval.

through multiple mechanisms<sup>46</sup>. For example, extended breeding seasons could lead to increased multiple brooding<sup>47</sup> or facilitate extended parental care, which could increase overwinter survival of juveniles<sup>48</sup>. The diverse range of possible outcomes highlights the increased need to study the relationship between migration phenology and breeding phenology<sup>49</sup>, particularly over large spatial and taxonomic scales. Differential shifts in phenology may also alter interspecific competition dynamics, which may have negative demographic consequences for some species<sup>50</sup>.

These findings regarding spatial and taxonomic variation in sensitivity also have implications for interpreting other widespread global change-driven phenomena, such as species' range shifts. As bird species are shifting both their winter and breeding distributions poleward over time<sup>33</sup>, a critical metric is the relative shift across seasons. In both Europe and North America, winter distributions are shifting faster than breeding distributions, leading to shortening of migratory distances<sup>33,51</sup>. Particularly if these shifts lead to transcontinental migrants switching to intracontinental migration—for example, by wintering along the coast of the Gulf of Mexico, as is increasingly seen in some species<sup>52</sup>—our findings indicate that this could lead to a renewed ability of some species to track advancing green-up (though unfilled habitat requirements may limit the potential for some range shifts). Such a phenomenon would be much-needed good news for neotropical migrants, which have seen dramatic population declines in recent years due to the cumulative effects of a diverse range of threats on both breeding and overwintering grounds<sup>14</sup>. Alternatively, since phenological changes may, in some situations, mitigate the need for range shifts<sup>53</sup>, species whose breeding phenology are more sensitive to changing climate may also shift their breeding distributions less.

Given variation in species' capacity to respond to and keep pace with rapid anthropogenic climate change, the ability to identify vulnerable species and at-risk landscapes will be necessary for the conservation of biodiversity and the effective management of natural resources. Previous studies have come to mixed conclusions

regarding how and why phenology is changing<sup>54</sup>, the implications these changes have for phenological mismatch<sup>55</sup> and which species characteristics might leave them more vulnerable to phenological change<sup>37</sup>. We present evidence to suggest why phenological sensitivity differs over space and across species. This species-specific, spatially explicit approach to estimating migratory arrival, in conjunction with other approaches such as the tracking of individual birds, will facilitate future work aimed at better understanding transcontinental avian phenological dynamics.

## Methods

To characterize changes in avian phenology and its sensitivity to spring arrival across time, space and species we developed a methodological pipeline that made use of observations from an expansive ornithological dataset and satellite-based remote sensors. We applied a hierarchical Bayesian analytical approach<sup>56</sup> to account for uncertainty and propagate it throughout the analyses, the specific details of which are outlined in following sections. We derived estimates of bird arrival by fitting logistic GAMs to checklist data collected by observers across eastern North America. We combined estimates from locales to generate region-wide estimates of arrival time by fitting a spatial autoregressive model to derive spatially smoothed estimates of phenology. Once we generated spatiotemporal estimates of arrival dates, we then used these estimates to fit a hierarchical spatially varying coefficients model to estimate how the effect of vegetation phenology (green-up) on bird phenology varies over space and across species. Due to theoretical and computational considerations, some parts of this pipeline are linked by treating marginal posterior distributions for parameters in one analysis as data in a downstream analysis (Extended Data Fig. 7 and Supplementary Table 2). Doing so allowed us to incorporate uncertainty into predictions at subsequent levels. Most phenological studies model the quantity of interest (often the first or mean date of a phenological observation<sup>57,58</sup>), failing to account for varying data collection effort both within and among years and ignoring uncertainty in these estimates. Here, we account for both varying effort and uncertainty in our phenological estimates and downstream analyses.

**Study region, dates, bird species and data sources.** We characterized bird migration phenology throughout eastern North America using data from Project eBird, an online community-science platform for bird observations<sup>15</sup>. We restricted the spatial scope of our analyses to the area of North America east of 95°W longitude and north of 24°N latitude to focus on the Eastern Temperate Forest biome and make use of the high density of bird observations in this area. To aggregate data within equal-sized areas large enough to allow robust estimates of phenology, we used a uniform hexagonal grid (Icosahedral Snyder Equal Area projection with an aperture of 3; distance between cell centres of 285 km; per-cell area of ~70,000 km<sup>2</sup>) which covered our study region (produced using the R package dggridR<sup>59</sup>; Extended Data Fig. 1). We limited the temporal scope of our analyses to the years 2002–2017. While some eBird observers have entered data based on field-notes made before 2002 (eBird's first year of operation), the volume of data is generally much lower. We focused analyses on migratory, forest- or near-forest-dwelling, primarily passerine birds that breed in eastern North America. From an initial list of 114 species, we ultimately analysed 56 species that met our data requirements (Extended Data Fig. 4; requirements outlined below), comprising one species of the order Caprimulgiformes, one from Cuculiformes and 54 from Passeriformes (Supplementary Table 1). For each species, we restricted analyses to grid cells within their breeding and migratory range (excluding areas where they overwinter), which we assessed using standard range maps<sup>60</sup>. We downloaded the eBird 'basic' dataset in December 2018 and extracted 'complete' checklists conducted before ordinal date (day-of-year) 200 (19 July in non-leap years), with a reported survey effort of between 6 min and 24 h, a reported distance <100 km and a start time before 18:00 local time (to exclude night-time surveys).

Estimates of spring vegetation phenology (green-up) from 2002 to 2017 were obtained from the Moderate Resolution Imaging Spectroradiometer (MODIS) Land Cover Dynamics MCD12Q2 v.6 data product<sup>16</sup> which corresponds well to independent field-derived phenological measurements<sup>57</sup>. MCD12Q2 product pixels (500 m) were filtered by land cover type, as characterized by the Land Cover Classification System from the Food and Agriculture Organization<sup>61</sup> provided as part of the MCD12Q1 v.6 data product<sup>62</sup>. The MCD12Q2 and MCD12Q1 products are produced on the same spatial grid allowing for easy filtering based on land cover classifications. Vegetation phenology values were only extracted for pixels classified as forest (evergreen needleleaf forests, evergreen broadleaf forests, deciduous needleleaf forests, deciduous broadleaf forests, mixed broadleaf/needleleaf forests, mixed broadleaf evergreen/deciduous forests, open forests or sparse forests) in the year 2017 as provided by the MCD12Q1 product and with vegetation phenology quality scores of 'good' or 'best', as provided by the MCD12Q2 product. Quantitative estimates of pixel-level green-up uncertainty are not available for this product. We selected 'mid-green-up' as our metric of green-up, which estimates the day of the year at which the amplitude of the modelled Enhanced Vegetation Index was half of its maximum<sup>16</sup>. The green-up

value for a given hexagonal grid cell for a given year was calculated as the mean of the green-up values for all pixels with appropriate land cover type and quality scores within that cell. Cell-level green-up values were only used if at least 10,000 valid pixels (~2,500 km<sup>2</sup>) were available to calculate the mean.

**Annualized, independent gridded estimates of migratory phenology.** We used presence/absence data from 7,150,883 bird observations contained in 2,068,687 unique eBird checklists to estimate annual arrival dates across the study area. We fit independent GAMs<sup>65</sup> in a Bayesian framework for each species–cell–year combination to estimate the half-maximum date, our metric of bird arrival in this study. This grid-based approach builds on previous analyses of interannual variation in migratory timing<sup>11,12</sup> but differs from other spatiotemporal exploratory models commonly fit to eBird data<sup>64</sup>, which have, thus far, not been able to resolve annualized phenology estimates due to high data requirements. The record of a given bird species in a checklist ( $y$ ) was modelled as a Bernoulli-distributed random variable (where a record is represented as a 1 and absence of a record is a 0), with the per-checklist reporting probability ( $p$ ) modelled as a logit-linear function of effort-hours (EH) and a penalized thin-plate regression spline<sup>65</sup> smoother for ordinal date (day-of-year)

$$y_i \sim \text{Bern}(p_i) \tag{1}$$

$$\text{logit}(p_i) = \alpha_{\text{GAM}} + \beta_{\text{GAM}} \times \text{EH}_i + f(\text{Day}_i)$$

where  $i$  is an individual checklist,  $\alpha_{\text{GAM}}$  is the intercept,  $\beta_{\text{GAM}}$  is the effect of EH, ‘Day’ is the ordinal date for a given checklist and  $f$  is a smooth function of Day. Our GAM-based approach contrasts with previous approaches of fitting parametric functions to the reporting frequency in eBird data as a function of Day<sup>11,12</sup>. Visual inspection of eBird checklist observations showed clear early-summer peaks in detection followed by declines in many cases. These nonlinear patterns are likely to interfere with estimating the height of the asymptote (and therefore the position of the half-maximum date) in the scaled logistic model (as used by previous studies). Given expected differences in migration patterns across species, as well as within species across their ranges, the functional form of the probability of occurrence in a checklist is also likely to vary across species and cells, particularly as a function of the relative proportion of phenological signal deriving from passage migrants versus local breeders<sup>66</sup>. We therefore used GAMs due to their flexibility in modelling a variety of functional forms and their recommendation in other phenological applications<sup>66</sup>.

We only fit GAMs in species–cell–years that met certain data conditions. For each species–cell–year, we required detections on at least ten unique days, at most 2% of detections occurring before day 60 (around 1 March) and non-detections on at least 20 unique days before the first detection. These threshold choices were based on results obtained during the exploratory phase of the analyses. We imposed the first requirement to avoid spurious spikes in the GAM in regions that are not well-constrained by data. We imposed the last two requirements to ensure that the species did not overwinter in substantial numbers within the cell and that early-season non-detections were sufficient to constrain the model to low values early in the season.

To calculate the half-maximum metric for a given species–cell–year, at each iteration of a posterior chain we calculated the first local maximum of the modelled per-checklist reporting probability to come after the first detection. The half-maximum was defined as the ordinal date at which the reporting probability is half the difference between the local maximum and minimum value plus the minimum reporting probability (Extended Data Fig. 2). In most cases, this corresponds to the ordinal date at which the reporting probability is half of the local maximum, although for some iterations, the minimum reporting probability before the local maximum may be non-negligibly >0. Half-maximum values for species–cell–years where no local maximum existed for >1% of posterior iterations (the second derivative of the reporting probability was never negative) were not used in downstream analyses (Extended Data Fig. 2). By calculating this derived half-maximum parameter at each iteration of the posterior chain, we obtained a posterior distribution of the half-maximum date, reflecting the uncertainty in this measure (Extended Data Fig. 2).

We fit the GAMs with a basis dimension ( $k$ ) of 30 in a Bayesian framework using the R package rstanarm<sup>67</sup> to interface with Stan<sup>68</sup>. We ran four chains for 1,500 iterations each with a warmup of 750 iterations. We assessed model convergence using the potential scale reduction factor (Rhat)<sup>69</sup> and number of effective samples. We discarded any species–cell–years with divergent transitions (which indicate that the sampler was not exploring probability space properly)<sup>68</sup>, Rhat > 1.02, number of effective samples <400 for any parameter or a posterior distribution for the half-maximum date with s.d. > 15 d. In total, we estimated valid half-maximum dates for 26,118 species–cell–year combinations.

**Smoothing and interpolation of phenology with spatial autoregressive models.**

We used the GAM-derived half-maximum estimates in conjunction with intrinsic autoregressive (IAR; also referred to as intrinsic conditional autoregressive, ICAR) models to derive more accurate phenological measures, leveraging the fact that the timing of bird migration is spatially autocorrelated within years. IAR models provide a framework to estimate the local dependency among variables in areal

data (data aggregated into discrete spatial units<sup>70,71</sup>). By quantifying the degree of spatial autocorrelation among variables, these models produce spatially smoothed estimates of those variables. For a given cell, the spatial random effect estimated by an IAR is dependent on the values of the neighbouring cells and the uncertainty in those values.

We constructed IAR models to estimate latent modelled arrival dates for each species–cell–year using the GAM-derived half-maximum estimates (with associated posterior uncertainty) as the response variable in these models. Our IAR models partially pooled data across cells and year but not across species (that is, we fit a separate model for each species). We fit IAR models only for species–year combinations with GAM estimates for arrival in at least three cells and only for species where at least 40% of the cells from the species’ migratory and breeding ranges that fell within the study area had at least 3 yr of data. While 40% was an arbitrary threshold, this choice was made to ensure that sensitivity estimates were available over a substantial portion of the species ranges. We also excluded data from cells where <5% of the cell was covered by land, as these values might reflect very localized (principally coastal) dynamics. Although rare, cells that had no neighbours were dropped from the analysis, as limited spatial information could be shared in these cases. In total, 56 species with 20,576 species–cell–years were used in the IAR analysis (Extended Data Fig. 4). We modelled the observed posterior mean of the GAM-derived half-maximum (HM) for cell  $i$  in year  $j$  as normally distributed, with the mean represented by the latent modelled arrival date (ARR) and s.d. represented by the uncertainty in the half-maximum estimate ( $\sigma_{\widehat{\text{HM}}}$ ; the posterior s.d. of the half-maximum estimate)

$$\widehat{\text{HM}}_{ij} \sim N(\text{ARR}_{ij}, \sigma_{\widehat{\text{HM}}_{ij}}) \tag{2}$$

In this way, the uncertainty in the estimate of the half-maximum is propagated through downstream analyses—GAM-derived half-maximum estimates with little uncertainty would tend not to differ greatly from IAR-derived estimates, while GAM-derived half-maximum estimates that were less precisely estimated draw more information from neighbouring estimates. We considered the modelled arrival of each species, ARR, as a function of a year effect ( $\beta_{\text{IAR}_j}$ , an offset in the arrival date for all cells in a given year), a cell effect ( $\gamma_{\text{IAR}_i}$ , an offset representing the typical arrival date for a cell across years) and a within-year spatial random effect ( $\phi_{\text{IAR}} \times \sigma_{\phi_{\text{IAR}}}$ , where  $\phi_{\text{IAR}}$  is the spatial effect scaled to 1 s.d. (for computational efficiency) and  $\sigma_{\phi_{\text{IAR}}}$  regulates the magnitude of that spatial effect for all years), with process error  $\sigma_{\text{ARR}}$

$$\text{ARR}_{ij} \sim N(\mu_{\text{ARR}_{ij}}, \sigma_{\text{ARR}}) \tag{3}$$

$$\mu_{\text{ARR}_{ij}} = \beta_{\text{IAR}_j} + \gamma_{\text{IAR}_i} + \phi_{\text{IAR}_{ij}} \times \sigma_{\phi_{\text{IAR}}}$$

$\beta_{\text{IAR}}$  was modelled as normally distributed with mean 0, s.d.  $\sigma_{\beta_{\text{IAR}}}$

$$\beta_{\text{IAR}_j} \sim N(0, \sigma_{\beta_{\text{IAR}}}) \tag{4}$$

To leverage the universal pattern of northward progression of spring migration, we modelled the cell effect ( $\gamma_{\text{IAR}}$ ) as a linear function of latitude

$$\gamma_{\text{IAR}_i} \sim N(\mu_{\gamma_{\text{IAR}_i}}, \sigma_{\gamma_{\text{IAR}_i}}) \tag{5}$$

$$\mu_{\gamma_{\text{IAR}_i}} = \alpha_{\gamma_{\text{IAR}}} + \beta_{\gamma_{\text{IAR}}} \times \text{LAT}_i$$

where  $\alpha_{\gamma_{\text{IAR}}}$  is the intercept,  $\beta_{\gamma_{\text{IAR}}}$  is the effect of latitude, LAT is the latitude of the centroid of cell  $i$  and  $\sigma_{\gamma_{\text{IAR}_i}}$  is the process error.

The spatial random effect  $\phi_{\text{IAR}}$  represents the degree to which each cell is augmented due to values of neighbouring cells and is defined as

$$\phi_{\text{IAR}} \sim N(0, [D - W]^{-1}) \tag{6}$$

where  $D$  is a diagonal matrix, with the number of neighbours for each cell on the diagonal and 0 on the off-diagonal elements and  $W$  is the weights matrix, with a binary encoding representing the proximity of two cells (taken from the spatial structure of the hex cells that represent a given species’ migratory and breeding range), such that  $w_{m,n} = 1$  if cell  $m$  is adjacent to cell  $n$  and  $w_{m,n} = 0$  otherwise. We formulate the spatial component  $\phi_{\text{IAR}}$  using the pairwise difference formula<sup>72</sup>. The model was parameterized such that the spatial structure of the autocorrelation was estimated independently for each year but a single parameter,  $\sigma_{\phi_{\text{IAR}}}$ , scaled the magnitude of this autocorrelation for all years for each species. The log probability density of  $\phi_{\text{IAR}}$  can be written as

$$\log p(\phi_{\text{IAR}}) = -\frac{1}{2} \left( \sum_{m \sim n} (\phi_{\text{IAR}_m} - \phi_{\text{IAR}_n})^2 \right) \tag{7}$$

A sum-to-zero constraint is necessary to ensure parameter identifiability in IAR models<sup>72</sup>

$$\sum_i \phi_{\text{IAR}_i} = 0 \tag{8}$$

We fit the IAR and all following models using R package rstan<sup>73</sup> to interface with Stan<sup>68</sup> in R<sup>74</sup>. For each model, we ran four chains for 5,000 iterations each with a warmup of 2,500 iterations. In cases where Rhat  $\geq 1.02$  or the number of effective samples for any parameter was  $< 400$ , the number of total and warmup iterations was doubled (up to a maximum of 40,000 total iterations) and the model was refit. Any model that failed to reach the specified Rhat and number of effective sample thresholds was discarded. No models had divergent transitions<sup>68</sup>. For all models, we implemented non-centred parameterizations of hierarchical parameters to increase the computational efficiency of model fitting in Stan<sup>75</sup>. Weakly informative priors were given for all parameters. Graphical posterior predictive checks were used to check that data generated by the model were similar to the data used to fit the model<sup>76</sup>. Data simulated from the posterior predictive distribution were similar to the observed data.

**Assessing species-level differences in bird arrival phenology as a function of green-up.** To characterize the sensitivity of bird arrival to changes in vegetation phenology, we modelled estimated arrival dates (ARR; the posterior mean of ARR (equation (2)), derived from the arrival IAR model) and their uncertainty as a function of green-up in a single hierarchical model for all species. ARR for cell  $i$ , year  $j$  and species  $k$  was modelled as normally distributed, with mean  $\mu_{\text{ARR}_{ijk}}$  and s.d.  $\sigma_{\text{ARR}_{ijk}}$  (the posterior s.d. of ARR (equation (2)), derived from the arrival IAR model). In this way, the uncertainty in the arrival estimates is propagated through the analyses. Only arrival dates in species–cells–years for which GAM-derived half-maximum values were estimated were used for these analyses (that is, no values interpolated by the arrival IAR model were used in downstream analyses). In total, 56 species and 20,576 species–cell–years were modelled. Green-up was standardized within each species–cell to have a mean of 0, as we were interested in the response of arrival to interannual fluctuations in green-up within a given area and the number of years where data were available for a given cell varied by species. All species were modelled jointly, so as to improve parameter estimation through partial pooling<sup>77</sup>

$$\begin{aligned}\widehat{\text{ARR}}_{ijk} &\sim N(\mu_{\text{ARR}_{ijk}}, \sigma_{\text{ARR}_{ijk}}) \\ \mu_{\text{ARR}_{ijk}} &\sim N(\mu_{\text{APG}_{jk}}, \sigma_{\text{APG}}) \\ \mu_{\text{APG}_{jk}} &= \alpha_{\text{APG}_{jk}} + \beta_{\text{APG}_{jk}} \times \text{CG}_{ijk}\end{aligned}\quad (9)$$

where  $\alpha_{\text{APG}}$  is the intercept term,  $\beta_{\text{APG}}$  is the effect of green-up on arrival, CG is green-up centred within each cell for each species,  $\sigma_{\text{APG}}$  is the process error and the APG subscript abbreviates ‘arrival days per green-up day’ (to help distinguish these parameters from those in other models). Separate slope and intercept parameters were estimated for each species–cell and modelled hierarchically as follows. Parameter  $\alpha_{\text{APG}}$  was modelled as a function of latitude, to leverage the fact that bird arrival occurs later at more northerly latitudes

$$\begin{aligned}\alpha_{\text{APG}_{ik}} &\sim N(\mu_{\alpha_{\text{APG}_{ik}}}, \sigma_{\alpha_{\text{APG}}}) \\ \mu_{\alpha_{\text{APG}_{ik}}} &= \pi_{\text{APG}_{ik}} + \nu_{\text{APG}_{ik}} \times \text{LAT}_i \\ \begin{bmatrix} \pi_{\text{APG}_{ik}} \\ \nu_{\text{APG}_{ik}} \end{bmatrix} &\sim \text{MVN} \left( \begin{bmatrix} \mu_{\pi_{\text{APG}}} \\ \mu_{\nu_{\text{APG}}} \end{bmatrix}, \Sigma_{\text{APG}} \right)\end{aligned}\quad (10)$$

where  $\pi_{\text{APG}}$  is the intercept term for  $\alpha_{\text{APG}}$  and  $\nu_{\text{APG}}$  is the effect of latitude on  $\alpha_{\text{APG}}$ , LAT is the latitude at the centroid of cell  $i$  and  $\sigma_{\alpha_{\text{APG}}}$  is the process error. Parameters  $\pi_{\text{APG}}$  and  $\nu_{\text{APG}}$  were modelled as multivariate normal, with means  $\mu_{\pi_{\text{APG}}}$  and  $\mu_{\nu_{\text{APG}}}$ , respectively, and covariance  $\Sigma_{\text{APG}}$  (a  $2 \times 2$  covariance matrix). Parameter  $\beta_{\text{APG}}$  was modelled as a function of latitude (with slope  $\gamma_{\text{APG}}$ , to examine the effect of latitude on the species-level sensitivity to green-up), a species-level intercept for the rate of change ( $\xi_{\text{APG}}$ ) and a spatial random effect ( $\phi_{\text{APG}}$  scaled by  $\sigma_{\phi_{\text{APG}}}$ ), to account for the fact that sensitivity to green-up is likely to be similar among nearby cells for a given species

$$\begin{aligned}\beta_{\text{APG}_{ik}} &\sim N(\mu_{\beta_{\text{APG}_{ik}}}, \sigma_{\beta_{\text{APG}}}) \\ \mu_{\beta_{\text{APG}_{ik}}} &= \xi_{\text{APG}_{ik}} + \gamma_{\text{APG}_{ik}} \times \text{SL}_{ik} + \phi_{\text{APG}_{ik}} \times \sigma_{\phi_{\text{APG}_{ik}}}\end{aligned}\quad (11)$$

where  $\sigma_{\beta_{\text{APG}}}$  represents the process error and SL represents latitude standardized within species, so  $\xi_{\text{APG}}$  represents the sensitivity to green-up (number of days change in arrival at a given cell per one-day change in green-up) for species  $k$  at the mean latitude of the species’ migratory and breeding range. This model used an IAR structure similar to models of arrival phenology but puts the spatial random effect on the rate of change over time rather than the phenological estimate (sometimes referred to as a spatially varying coefficients model<sup>78</sup>).

To assess why species differed in their sensitivity to green-up, we modelled  $\xi_{\text{APG}}$  as a function of species-level migratory traits: migration pace (the number of days on average that a species takes to cover one degree latitude during migration), arrival date (the mean date over a species’ migratory and breeding range across all years) and overwinter latitude (the latitude of the centroid of the species’

overwinter range). Since these traits covary (correlation coefficients: migration pace and arrival date,  $-0.51$ ; migration pace and overwinter latitude,  $0.40$ ; mean arrival date and overwinter latitude,  $-0.39$ ), we regressed species-level sensitivity to green-up on the first principal component (PC1) of these three variables (which represents 62% of the variation in these variables; Supplementary Table 3) to avoid issues of multicollinearity

$$\begin{aligned}\xi_{\text{APG}_{ik}} &\sim N(\mu_{\xi_{\text{APG}_{ik}}}, \sigma_{\xi_{\text{APG}}}) \\ \mu_{\xi_{\text{APG}_{ik}}} &= \alpha_{\xi} + \beta_{\xi} \times \text{PC1}_k\end{aligned}\quad (12)$$

where  $\alpha_{\xi}$  is the intercept term,  $\beta_{\xi}$  is the effect of PC1 and  $\sigma_{\xi_{\text{APG}}}$  is the process error. Parameter  $\beta_{\xi_{\text{IAR}}}$  (equation (5); representing the effect of latitude on the cell random effect in days per degree latitude) from the IAR model was used as a measure of migration pace. We represented species-level overwinter latitude as the centroid of the species’ overwinter range, as determined from published range maps<sup>40</sup>. Mean arrival date was calculated as the mean estimated arrival date for all cells across the species’ migratory and breeding ranges across all years. While this measure of migration pace and estimates of arrival phenology are derived from the same model, migration pace is estimated in such a way that it has little to do with either the average arrival date for each species or how much arrival date might vary from year to year.

$\gamma_{\text{APG}}$  (the effect of latitude on the species-level sensitivity to green-up) was modelled as hierarchically normally distributed

$$\gamma_{\text{APG}_{ik}} \sim N(\mu_{\gamma_{\text{APG}}}, \sigma_{\gamma_{\text{APG}}})\quad (13)$$

with mean  $\mu_{\gamma_{\text{APG}}}$  and s.d.  $\sigma_{\gamma_{\text{APG}}}$ .

Because migratory and breeding ranges varied across species, separate adjacency matrices were created for each species to estimate the spatial random effect. Parameter  $\sigma_{\phi_{\text{APG}}}$  was modelled hierarchically, to aid in estimation across species. A log normal distribution was used to allow for a non-centred parameterization<sup>79</sup> of a zero-bounded parameter

$$\sigma_{\phi_{\text{APG}_{ik}}} \sim \text{LN}(\lambda_{\text{APG}}, \kappa_{\text{APG}})\quad (14)$$

where  $\lambda_{\text{APG}}$  is the location parameter and  $\kappa_{\text{APG}}$  is the scale parameter. We ran four chains for 7,000 iterations and discarded the initial 3,000 iterations as warmup. Graphical posterior predictive checks showed that data simulated from the posterior predictive distribution were similar to the observed data (Extended Data Fig. 8).

The proportion of within-cell variation in arrival explained by green-up was assessed as

$$\frac{\text{var}(\mu_{\text{APG}_{ik}})}{\text{var}(\mu_{\text{ARR}_{ik}})}\quad (15)$$

where  $\mu_{\text{APG}}$  is the linear predictor (equation (9)) and  $\mu_{\text{ARR}}$  is the total variance of predicted arrival dates (equation (9)) for each species–cell at each iteration of the posterior. This was calculated at each iteration of the posterior chain. The median across all iterations was calculated for each species–cell to quantify the proportion of within-cell variation explained by green-up. Species-level means were calculated by taking the mean of these medians for each species. The overall within-cell variation explained by green-up was taken as the mean of these species-level means.

**Sensitivity as a function of interannual variation in arrival.** To determine to what degree species-level sensitivity in arrival was related to flexibility in interannual arrival, we calculated the correlation between  $\xi_{\text{APG}}$  (species-level sensitivity of bird arrival to green-up; equation (11)) and a derived quantity,  $\sigma_{\mu}$  (species-level interannual variability in arrival date). To calculate the derived quantity,  $\sigma_{\mu}$ , we first calculated  $\delta$ , the difference between  $\mu_{\text{ARR}}$  (the latent arrival date for each species–cell–year; equation (9)) and  $\alpha_{\text{APG}}$  (the cell intercept for each species–cell; equation (9)) for each species–cell–year, at each iteration of the posterior chain

$$\delta_{ijk} = \mu_{\text{ARR}_{ijk}} - \alpha_{\text{APG}_{ik}}\quad (16)$$

This quantity represents centred (for each species–cell) bird arrival dates. We then calculated  $\sigma_{\mu}$  as the s.d. of each realization of  $\delta$  (where the number of realizations is equal to the number of posterior iterations for  $\mu_{\text{ARR}}$  and  $\alpha_{\text{APG}}$ ) for each species

$$\sigma_{\mu_k} = \text{s.d.}(\delta_k)\quad (17)$$

yielding a derived posterior distribution representing the degree of interannual variability in arrival dates for each species. We then calculated correlation coefficients between  $\xi_{\text{APG}}$  and  $\sigma_{\mu}$  at each realization of the posteriors

$$\rho = \text{cor}(\xi_{\text{APG}_k}, \sigma_{\mu_k})\quad (18)$$

to compare species-level sensitivity to species-level interannual variability. This resulted in a distribution of correlation coefficients, on which we then made inference.

**Estimating trends in green-up over time.** To characterize changes in forest green-up phenology, we modelled the green-up date (GR) (the ‘mid-green-up’ metric from the MCD12Q2 product<sup>16</sup>) for cell  $i$  in year  $j$  as a linear function of time (YEAR)

$$\begin{aligned} \text{GR}_{ij} &\sim N(\mu_{\text{GR}_j}, \sigma_{\text{GR}}) \\ \mu_{\text{GR}_j} &= \alpha_{\text{GR}_i} + \beta_{\text{GR}_i} \times \text{YEAR}_j \end{aligned} \quad (19)$$

where  $\alpha_{\text{GR}}$  is the intercept term,  $\beta_{\text{GR}}$  is the rate of phenological change over time (YEAR) and  $\sigma_{\text{GR}}$  is the process error. Separate slope and intercept parameters were estimated for each cell and modelled hierarchically as follows. Parameter  $\alpha_{\text{GR}}$  was modelled as a linear function of latitude, to leverage the fact that green-up occurs later in the year at more northerly latitudes

$$\begin{aligned} \alpha_{\text{GR}_i} &\sim N(\mu_{\alpha_{\text{GR}_i}}, \sigma_{\alpha_{\text{GR}}}) \\ \mu_{\alpha_{\text{GR}_i}} &= \pi_{\text{GR}} + \nu_{\text{GR}} \times \text{LAT}_i \end{aligned} \quad (20)$$

where  $\pi_{\text{GR}}$  is the intercept term,  $\nu_{\text{GR}}$  is the effect of latitude on  $\alpha_{\text{GR}}$ , LAT is latitude at the centroid of cell  $i$  and  $\sigma_{\alpha_{\text{GR}}}$  is the process error.

The temporal trend in green-up phenology for each cell ( $\beta_{\text{GR}}$ ) was modelled as a function of an intercept ( $\xi_{\text{GR}}$ ) and a spatial random effect ( $\phi_{\text{GR}}$  scaled by  $\sigma_{\phi_{\text{GR}}}$ ), to account for the fact that the rate of change in green-up is likely to be similar among cells

$$\begin{aligned} \beta_{\text{GR}_i} &\sim N(\mu_{\beta_{\text{GR}_i}}, \sigma_{\beta_{\text{GR}}}) \\ \mu_{\beta_{\text{GR}_i}} &= \xi_{\text{GR}} + \phi_{\text{GR}_i} \times \sigma_{\phi_{\text{GR}}} \end{aligned} \quad (21)$$

This spatially varying coefficients structure of equation (21) is similar to equation (11), above. In total, 1,696 cell-years were modelled. We ran four chains for 8,000 iterations with a warmup of 4,000 iterations. We fit two separate models, one using green-up values from only forest land cover type and one using green-up values from all land cover types. Graphical posterior predictive checks showed that data simulated from the posterior predictive distribution were similar to the observed data (Extended Data Fig. 8). It should be noted that the spatial structure of the rate of change in green-up is land cover dependent, with middle latitudes of North America showing no trends in green-up when all land cover types are included (Extended Data Fig. 6), possibly resulting from the phenological insensitivity of agricultural practices<sup>90</sup>.

We fit models on the University of Connecticut’s Xanadu high-performance computing cluster and an Apple iMac desktop computer. In total, model fitting required ~1,240 processor-days of computing time.

**Reporting Summary.** Further information on research design is available in the Nature Research Reporting Summary linked to this article.

## Data availability

Bird occurrence data are available through eBird (<https://ebird.org>). Green-up (MCD12Q2) and land cover (MCD12Q1) data are available through the NASA/USGS Land Processes Distributed Active Archive Center (<https://lpdaac.usgs.gov/>). Interactive visualizations of all major analyses, as well as download capabilities of data products, are viewable on our R Shiny site at <https://migratory-sensitivity.shinyapps.io/MigSen-app/> which is also available on Github ([https://github.com/br-amara/MigratorySensitivity\\_ShinyApp](https://github.com/br-amara/MigratorySensitivity_ShinyApp)) and archived on Zenodo (<https://doi.org/10.5281/zenodo.4549910>).

## Code availability

Code used to derive the arrival estimates and conduct the analyses of phenological sensitivity are available on Github ([https://github.com/phenomismatch/Bird\\_Phenology](https://github.com/phenomismatch/Bird_Phenology); [https://github.com/caseyoungflesh/Pheno\\_sensitivity](https://github.com/caseyoungflesh/Pheno_sensitivity)) and archived on Zenodo (<https://doi.org/10.5281/zenodo.4532885>; <https://doi.org/10.5281/zenodo.4532799>).

Received: 16 September 2020; Accepted: 4 March 2021;

Published online: 29 April 2021

## References

- Parmesan, C. & Yohe, G. A globally coherent fingerprint of climate change impacts across natural systems. *Nature* **421**, 37–42 (2003).
- Cohen, J. M., Lajeunesse, M. J. & Rohr, J. R. A global synthesis of animal phenological responses to climate change. *Nat. Clim. Change* **8**, 224–228 (2018).

- Thackeray, S. J. et al. Phenological sensitivity to climate across taxa and trophic levels. *Nature* **535**, 241–245 (2016).
- Both, C., van Asch, M., Bijlsma, R. G., van den Burg, A. B. & Visser, M. E. Climate change and unequal phenological changes across four trophic levels: constraints or adaptations? *J. Anim. Ecol.* **78**, 73–83 (2009).
- Visser, M. E., van Noordwijk, A. J., Tinbergen, J. M. & Lessells, C. M. Warmer springs lead to mistimed reproduction in great tits (*Parus major*). *Proc. R. Soc. B* **265**, 1867–1870 (1998).
- Stenseth, N. C. & Mysterud, A. Climate, changing phenology, and other life history traits: nonlinearity and match–mismatch to the environment. *Proc. Natl Acad. Sci. USA* **99**, 13379–13381 (2002).
- Blackford, C., Germain, R. M. & Gilbert, B. Species differences in phenology shape coexistence. *Am. Nat.* **195**, E168–E180 (2020).
- Møller, A. P., Rubolini, D. & Lehikoinen, E. Populations of migratory bird species that did not show a phenological response to climate change are declining. *Proc. Natl Acad. Sci. USA* **105**, 16195–16200 (2008).
- Rudolf, V. H. W. The role of seasonal timing and phenological shifts for species coexistence. *Ecol. Lett.* **22**, 1324–1338 (2019).
- Mynott, J. *Birds in the Ancient World: Winged Words* (Oxford Univ. Press, 2018).
- Hurlbert, A. H. & Liang, Z. Spatiotemporal variation in avian migration phenology: citizen science reveals effects of climate change. *PLoS ONE* **7**, e31662 (2012).
- Mayor, S. J. et al. Increasing phenological asynchrony between spring green-up and arrival of migratory birds. *Sci. Rep.* **7**, 1902 (2017).
- Horton, K. G. et al. Phenology of nocturnal avian migration has shifted at the continental scale. *Nat. Clim. Change* **10**, 63–68 (2020).
- Rosenberg, K. V. et al. Decline of the North American avifauna. *Science* **366**, 120–124 (2019).
- Sullivan, B. L. et al. The eBird enterprise: an integrated approach to development and application of citizen science. *Biol. Conserv.* **169**, 31–40 (2014).
- Friedl, M., Gray, J. & Sulla-Menashe, D. *MCD12Q2 MODIS/Terra+ Aqua Land Cover Dynamics Yearly L3 Global 500m SIN Grid v.6* (NASA EOSDIS Land Processes DAAC, accessed 26 March 2020); <https://doi.org/10.5067/MODIS/MCD12Q2.006>
- Richardson, A. D., Hufkens, K., Milliman, T. & Froking, S. Intercomparison of phenological transition dates derived from the PhenoCam Dataset V1.0 and MODIS satellite remote sensing. *Sci. Rep.* **8**, 5679 (2018).
- Cole, E. F., Long, P. R., Zelazowski, P., Szulkin, M. & Sheldon, B. C. Predicting bird phenology from space: satellite-derived vegetation green-up signal uncovers spatial variation in phenological synchrony between birds and their environment. *Ecol. Evol.* **5**, 5057–5074 (2015).
- Pettorelli, N. et al. The normalized difference vegetation index (NDVI): unforeseen successes in animal ecology. *Clim. Res.* **46**, 15–27 (2011).
- Winger, B. M., Auteri, G. G., Pegan, T. M. & Weeks, B. C. A long winter for the Red Queen: rethinking the evolution of seasonal migration. *Biol. Rev.* **94**, 737–752 (2019).
- Åkesson, S. et al. Timing avian long-distance migration: from internal clock mechanisms to global flights. *Philos. Trans. R. Soc. B* **372**, 20160252 (2017).
- Helm, B. et al. Two sides of a coin: ecological and chronobiological perspectives of timing in the wild. *Philos. Trans. R. Soc. B* **372**, 20160246 (2017).
- Haest, B., Hüpopp, O. & Bairlein, F. The influence of weather on avian spring migration phenology: what, where and when? *Glob. Change Biol.* **24**, 5769–5788 (2018).
- Studds, C. E. & Marra, P. P. Rainfall-induced changes in food availability modify the spring departure programme of a migratory bird. *Proc. R. Soc. B* **278**, 3437–3443 (2011).
- Thorup, K. et al. Resource tracking within and across continents in long-distance bird migrants. *Sci. Adv.* **3**, e1601360 (2017).
- Post, E., Steinman, B. A. & Mann, M. E. Acceleration of phenological advance and warming with latitude over the past century. *Sci. Rep.* **8**, 3927 (2018).
- Van der Graaf, A., Stahl, J., Klimkowska, A., Bakker, J. P. & Drent, R. H. Surfing on a green wave—how plant growth drives spring migration in the Barnacle Goose *Branta leucopsis*. *Ardea Wagening.* **94**, 567 (2006).
- Schmaljohann, H. & Both, C. The limits of modifying migration speed to adjust to climate change. *Nat. Clim. Change* **7**, 573–576 (2017).
- Marra, P. P., Francis, C. M., Mulvihill, R. S. & Moore, F. R. The influence of climate on the timing and rate of spring bird migration. *Oecologia* **142**, 307–315 (2005).
- Zurell, D., Gallien, L., Graham, C. H. & Zimmermann, N. E. Do long-distance migratory birds track their niche through seasons? *J. Biogeogr.* **45**, 1459–1468 (2018).
- Horton, K. G. et al. Holding steady: little change in intensity or timing of bird migration over the Gulf of Mexico. *Glob. Change Biol.* **25**, 1106–1118 (2019).
- Charmantier, A. et al. Adaptive phenotypic plasticity in response to climate change in a wild bird population. *Science* **320**, 800–803 (2008).

33. Curley, S. R., Manne, L. L. & Veit, R. R. Differential winter and breeding range shifts: implications for avian migration distances. *Divers. Distrib.* **26**, 415–425 (2020).
34. Root, T. Energy constraints on avian distributions and abundances. *Ecology* **69**, 330–339 (1988).
35. La Sorte, F. A., Fink, D., Hochachka, W. M., DeLong, J. P. & Kelling, S. Population-level scaling of avian migration speed with body size and migration distance for powered fliers. *Ecology* **94**, 1839–1847 (2013).
36. Somveille, M., Manica, A. & Rodrigues, A. S. L. Where the wild birds go: explaining the differences in migratory destinations across terrestrial bird species. *Ecography* **42**, 225–236 (2019).
37. Knudsen, E. et al. Challenging claims in the study of migratory birds and climate change. *Biol. Rev.* **86**, 928–946 (2011).
38. Allstadt, A. J. et al. Spring plant phenology and false springs in the conterminous US during the 21st century. *Environ. Res. Lett.* **10**, 104008 (2015).
39. Franks, S. E. et al. The sensitivity of breeding songbirds to changes in seasonal timing is linked to population change but cannot be directly attributed to the effects of trophic asynchrony on productivity. *Glob. Change Biol.* **24**, 957–971 (2018).
40. Both, C., Bouwhuis, S., Lessells, C. M. & Visser, M. E. Climate change and population declines in a long-distance migratory bird. *Nature* **441**, 81–83 (2006).
41. Kharouba, H. M. & Wolkovich, E. M. Disconnects between ecological theory and data in phenological mismatch research. *Nat. Clim. Change* **10**, 406–415 (2020).
42. Samplonius, J. M. et al. Strengthening the evidence base for temperature-mediated phenological asynchrony and its impacts. *Nat. Ecol. Evol.* **5**, 155–164 (2021).
43. Abdala-Roberts, L. et al. Tri-trophic interactions: bridging species, communities and ecosystems. *Ecol. Lett.* **22**, 2151–2167 (2019).
44. Burgess, M. D. et al. Tritrophic phenological match–mismatch in space and time. *Nat. Ecol. Evol.* **2**, 970–975 (2018).
45. Helm, B., Van Doren, B. M., Hoffmann, D. & Hoffmann, U. Evolutionary response to climate change in migratory pied flycatchers. *Curr. Biol.* **29**, 3714–3719 (2019).
46. Newson, S. E. et al. Long-term changes in the migration phenology of UK breeding birds detected by large-scale citizen science recording schemes. *Ibis* **158**, 481–495 (2016).
47. Townsend, A. K. et al. The interacting effects of food, spring temperature, and global climate cycles on population dynamics of a migratory songbird. *Glob. Change Biol.* **22**, 544–555 (2016).
48. Gruebler, M. U. & Naef-Daenzer, B. Fitness consequences of pre- and post-fledging timing decisions in a double-brooded passerine. *Ecology* **89**, 2736–2745 (2008).
49. Lany, N. K. et al. Breeding timed to maximize reproductive success for a migratory songbird: the importance of phenological asynchrony. *Oikos* **125**, 656–666 (2016).
50. Samplonius, J. M. & Both, C. Climate change may affect fatal competition between two bird species. *Curr. Biol.* **29**, 327–331 (2019).
51. Potvin, D. A., Välimäki, K. & Lehikoinen, A. Differences in shifts of wintering and breeding ranges lead to changing migration distances in European birds. *J. Avian Biol.* **47**, 619–628 (2016).
52. Bassett, F. & Cubie, D. Wintering hummingbirds in Alabama and Florida: species diversity, sex and age ratios, and site fidelity. *J. Field Ornithol.* **80**, 154–162 (2009).
53. Socolar, J. B., Epanchin, P. N., Beissinger, S. R. & Tingley, M. W. Phenological shifts conserve thermal niches in North American birds and reshape expectations for climate-driven range shifts. *Proc. Natl Acad. Sci. USA* **114**, 12976–12981 (2017).
54. Chmura, H. E. et al. The mechanisms of phenology: the patterns and processes of phenological shifts. *Ecol. Monogr.* **89**, e01337 (2019).
55. Kharouba, H. M. et al. Global shifts in the phenological synchrony of species interactions over recent decades. *Proc. Natl Acad. Sci. USA* **115**, 5211–5216 (2018).
56. Cressie, N., Calder, C. A., Clark, J. S., Hoef, J. M. V. & Wikle, C. K. Accounting for uncertainty in ecological analysis: the strengths and limitations of hierarchical statistical modeling. *Ecol. Appl.* **19**, 553–570 (2009).
57. Miller-Rushing, A. J., Inouye, D. W. & Primack, R. B. How well do first flowering dates measure plant responses to climate change? The effects of population size and sampling frequency. *J. Ecol.* **96**, 1289–1296 (2008).
58. Miller-Rushing, A. J., Lloyd-Evans, T. L., Primack, R. B. & Sazinger, P. Bird migration times, climate change, and changing population sizes. *Glob. Change Biol.* **14**, 1959–1972 (2008).
59. Barnes, R. dggridR: Discrete global grids for R. R package version 0.1.12 <https://github.com/r-barnes/dggridR> (2017).
60. *Data Zone* (BirdLife International, 2019); <http://datazone.birdlife.org/species/requestdis>
61. Sulla-Menashe, D. et al. Hierarchical mapping of Northern Eurasian land cover using MODIS data. *Remote Sens. Environ.* **115**, 392–403 (2011).
62. Friedl, M. & Sulla-Menashe, D. *MCD12Q1 MODIS/Terra+ Aqua Land Cover Type Yearly L3 Global 500m SIN Grid v6* (NASA EOSDIS Land Processes DAAC, accessed 26 February 2020); <https://doi.org/10.5067/MODIS/MCD12Q2.006>
63. Wood, S. N. & Augustin, N. H. GAMs with integrated model selection using penalized regression splines and applications to environmental modelling. *Ecol. Model.* **157**, 157–177 (2002).
64. Fink, D. et al. Spatiotemporal exploratory models for broad-scale survey data. *Ecol. Appl.* **20**, 2131–2147 (2010).
65. Wood, S. N. Thin plate regression splines. *J. R. Stat. Soc. B* **65**, 95–114 (2003).
66. Lindén, A., Meller, K. & Knappe, J. An empirical comparison of models for the phenology of bird migration. *J. Avian Biol.* **48**, 255–265 (2017).
67. Goodrich, B., Gabry, J., Ali, I. & Brilleman, S. rstanarm: Bayesian applied regression modeling via Stan. R package version 2.21.1 <https://mc-stan.org/rstanarm> (2020).
68. Carpenter, B. et al. Stan: a probabilistic programming language. *J. Stat. Softw.* <https://www.jstatsoft.org/v076/i01> (2017).
69. Brooks, S. P. & Gelman, A. General methods for monitoring convergence of iterative simulations. *J. Comput. Graph. Stat.* **7**, 434 (1998).
70. Besag, J. & Kooperberg, C. On conditional and intrinsic autoregression. *Biometrika* **82**, 733 (1995).
71. Banerjee, S., Carlin, B. P. & Gelfand, A. E. *Hierarchical Modeling and Analysis for Spatial Data* (Chapman & Hall/CRC, 2004).
72. Morris, M. et al. Bayesian hierarchical spatial models: implementing the Besag York Mollie model in stan. *Spat. Spatiotemporal Epidemiol.* **31**, 100301 (2019).
73. Stan Development Team. RStan: the R interface to Stan. R package version 2.17.3 <http://mc-stan.org> (2018).
74. R Core Team. *R: A Language and Environment for Statistical Computing* (R Foundation for Statistical Computing, 2019).
75. Monnahan, C. C., Thorson, J. T. & Branch, T. A. Faster estimation of Bayesian models in ecology using Hamiltonian Monte Carlo. *Methods Ecol. Evol.* **8**, 339–348 (2017).
76. Gabry, J., Simpson, D., Vehtari, A., Betancourt, M. & Gelman, A. Visualization in Bayesian workflow. *J. R. Stat. Soc. A* **182**, 389–402 (2019).
77. Gelman, A., Carlin, J. B., Stern, H. S. & Rubin, D. B. *Bayesian Data Analysis* (Chapman & Hall/CRC, 2014).
78. Finley, A. O. Comparing spatially-varying coefficients models for analysis of ecological data with non-stationary and anisotropic residual dependence: spatially-varying coefficients models. *Methods Ecol. Evol.* **2**, 143–154 (2011).
79. Stan Modeling Language Users Guide and Reference Manual v. 2.18.0 (Stan Development Team, 2018).
80. Menzel, A., von Vopelius, J., Estrella, N., Schleip, C. & Dose, V. Farmers' annual activities are not tracking the speed of climate change. *Clim. Res.* **32**, 201–207 (2006).

## Acknowledgements

Funding for this project was provided by the National Science Foundation (grant nos. EF 1703048 to M.W.T., 1702708 to A.H.H. and 2033263 to M.W.T.). M. Belitz, G. Di Cecco, E. Larsen, N. Neupane, L. Ries and J. Withey provided assistance and made suggestions that improved the paper. S. MacLean provided bird illustrations. We are grateful to the tens of thousands of eBird users who submit data each year.

## Author contributions

C.Y., J.S. and M.W.T. led conceptualization, formal analysis and writing of the original draft, with methodological, investigative and data curation support from A.A., R.P.G., A.H.H., R.L., S.J.M. and D.A.W.M. B.R.A. provided software and visualization support. The research project and supportive funding is administered by M.W.T. and A.H.H. All authors contributed to review and editing of drafts.

## Competing interests

The authors declare no competing interests.

## Additional information

**Extended data** is available for this paper at <https://doi.org/10.1038/s41559-021-01442-y>.

**Supplementary information** The online version contains supplementary material available at <https://doi.org/10.1038/s41559-021-01442-y>.

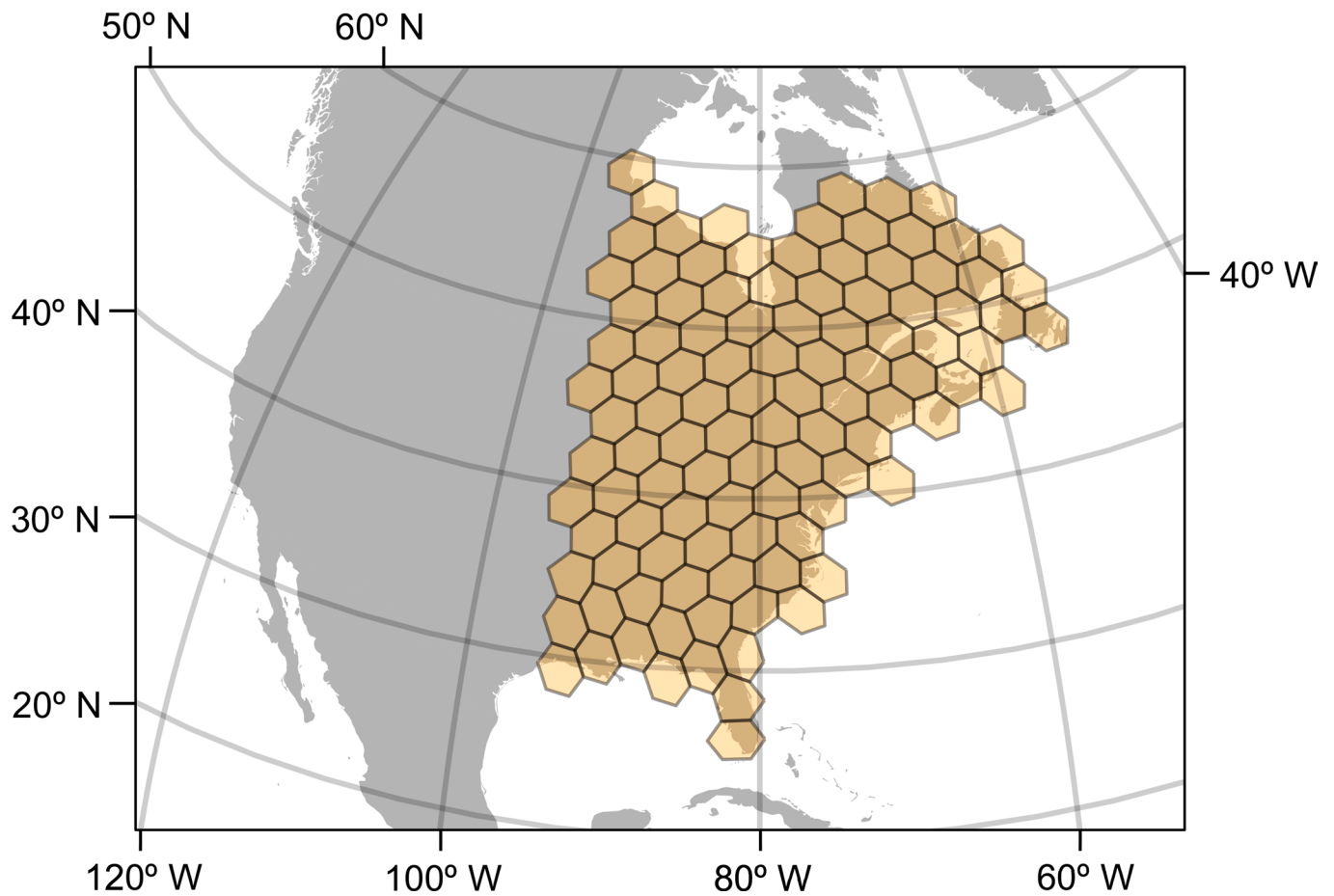
**Correspondence and requests for materials** should be addressed to M.W.T.

**Peer review information** *Nature Ecology & Evolution* thanks Adriaan Dokter, Albert Phillimore and the other, anonymous, reviewer(s) for their contribution to the peer review of this work. Peer reviewer reports are available.

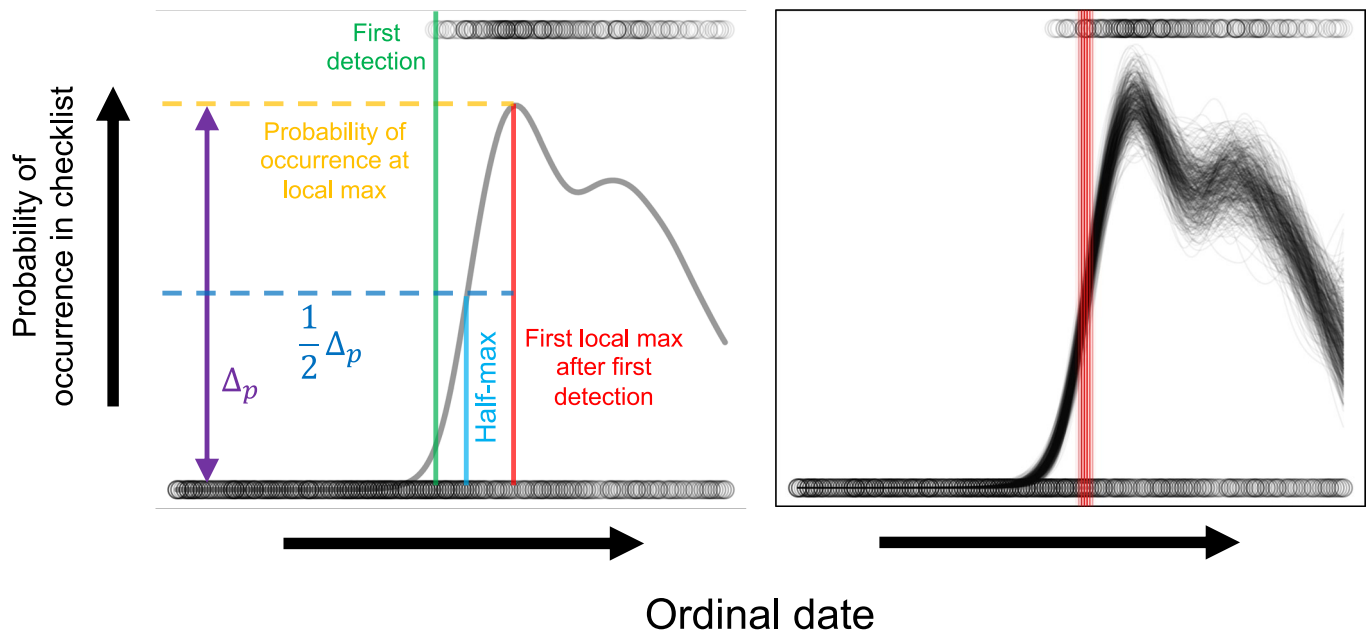
**Reprints and permissions information** is available at [www.nature.com/reprints](http://www.nature.com/reprints).

**Publisher's note** Springer Nature remains neutral with regard to jurisdictional claims in published maps and institutional affiliations.

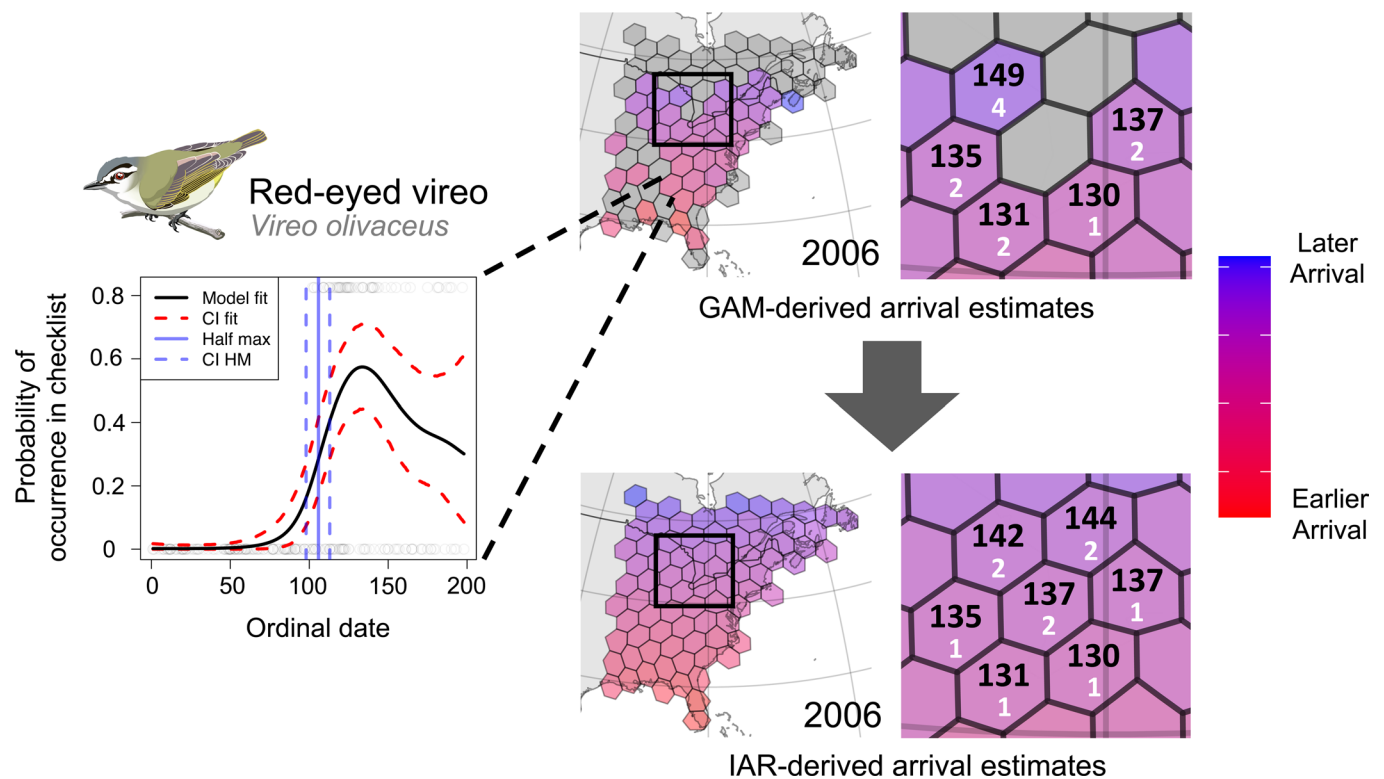
© The Author(s), under exclusive licence to Springer Nature Limited 2021



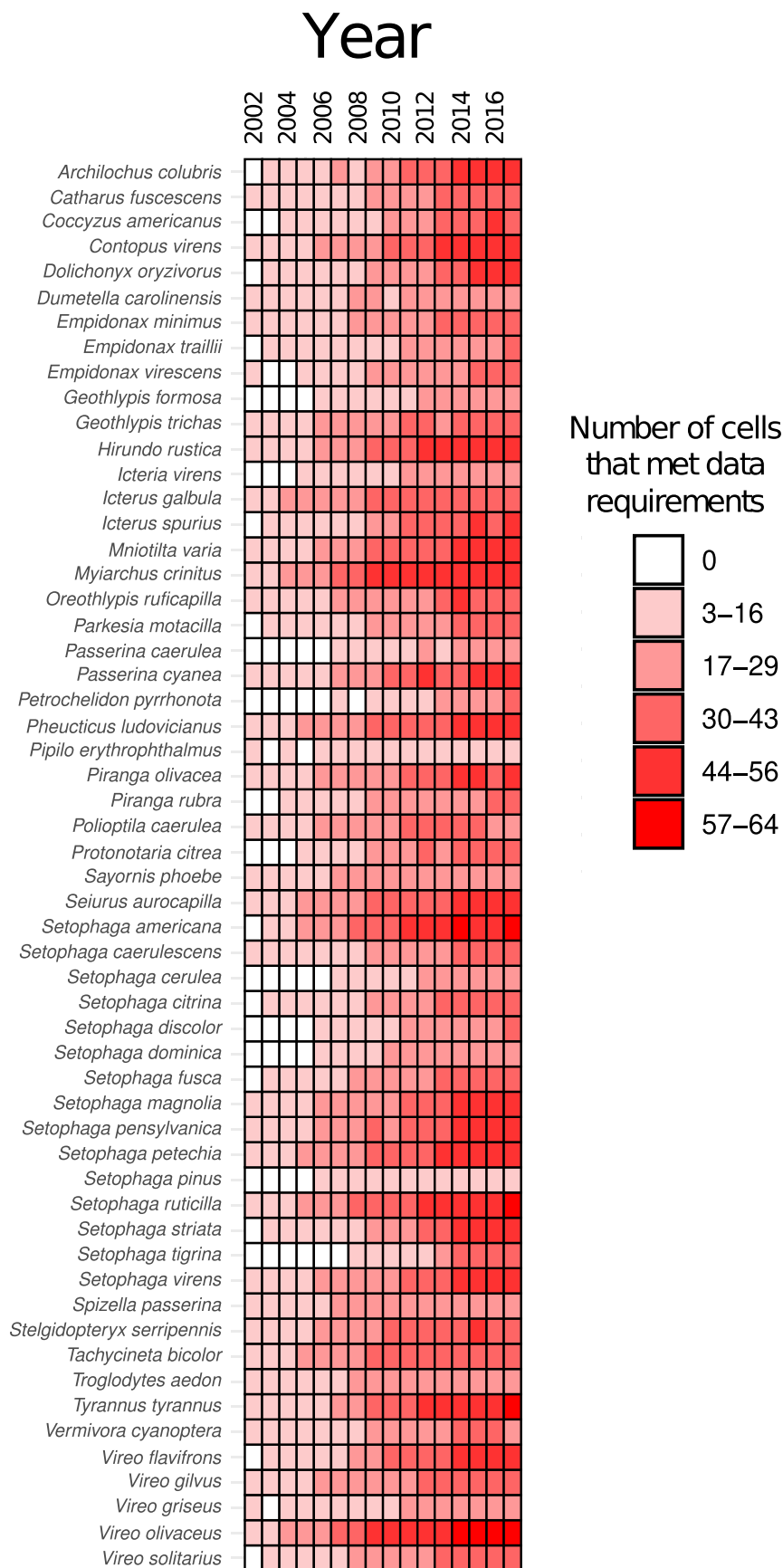
**Extended Data Fig. 1 | Study area of interest over North America.** Data were aggregated within each cell to calculate phenological measures and to characterize phenological change and sensitivity. Yellow cells represent the full extent of the study area. Cells were selected based on data density for both bird and green-up phenology (see Methods). Cell centres ranged from approximately 95° W to 54° W longitude and 26° N to 59° N latitude.



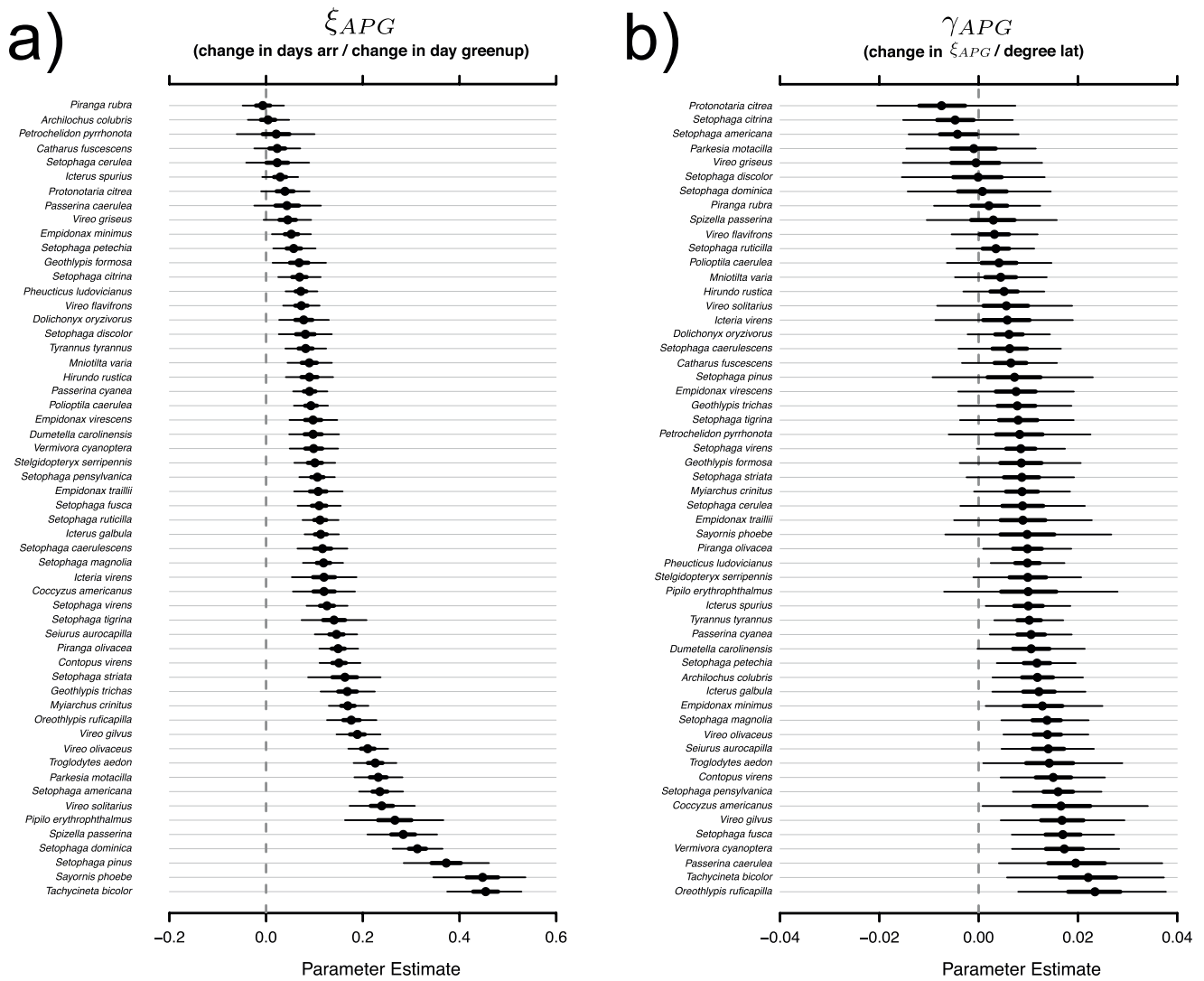
**Extended Data Fig. 2 | Derivation of the half-maximum from GAM results for each species-cell-year.** Circles at the top of each plot represent checklists where the species of interest was recorded, while circles at the bottom of each plot represent checklists where the species of interest was not recorded. Left panel: the green line represents the first detection of a given species in a given cell-year; the red line represents the first local maximum for the modelled probability of occurrence in an eBird checklist to come after the first detection; the gold line represents the probability of occurrence at that local maximum; the purple line represents  $\Delta_p$ , the difference between the minimum modelled probability of occurrence prior to the first local maximum and the probability of occurrence at the local maximum (the minimum reporting probability here is 0); the dark blue line represents the probability of occurrence at  $\frac{1}{2}\Delta_p$ , half the difference between the maximum and minimum probabilities plus the minimum reporting probability; the light blue line represents the half-maximum date, the ordinal date (day-of-year) at which the modelled probability of occurrence equals  $\frac{1}{2}\Delta_p$ . Right panel: black lines represent posterior realizations of the GAM model fit for a single species-cell-year (500 realizations shown for clarity). The red lines represent the derived half-maximum date at each realization of the GAM model fit and were used to calculate the mean and 95% credible intervals for this metric.



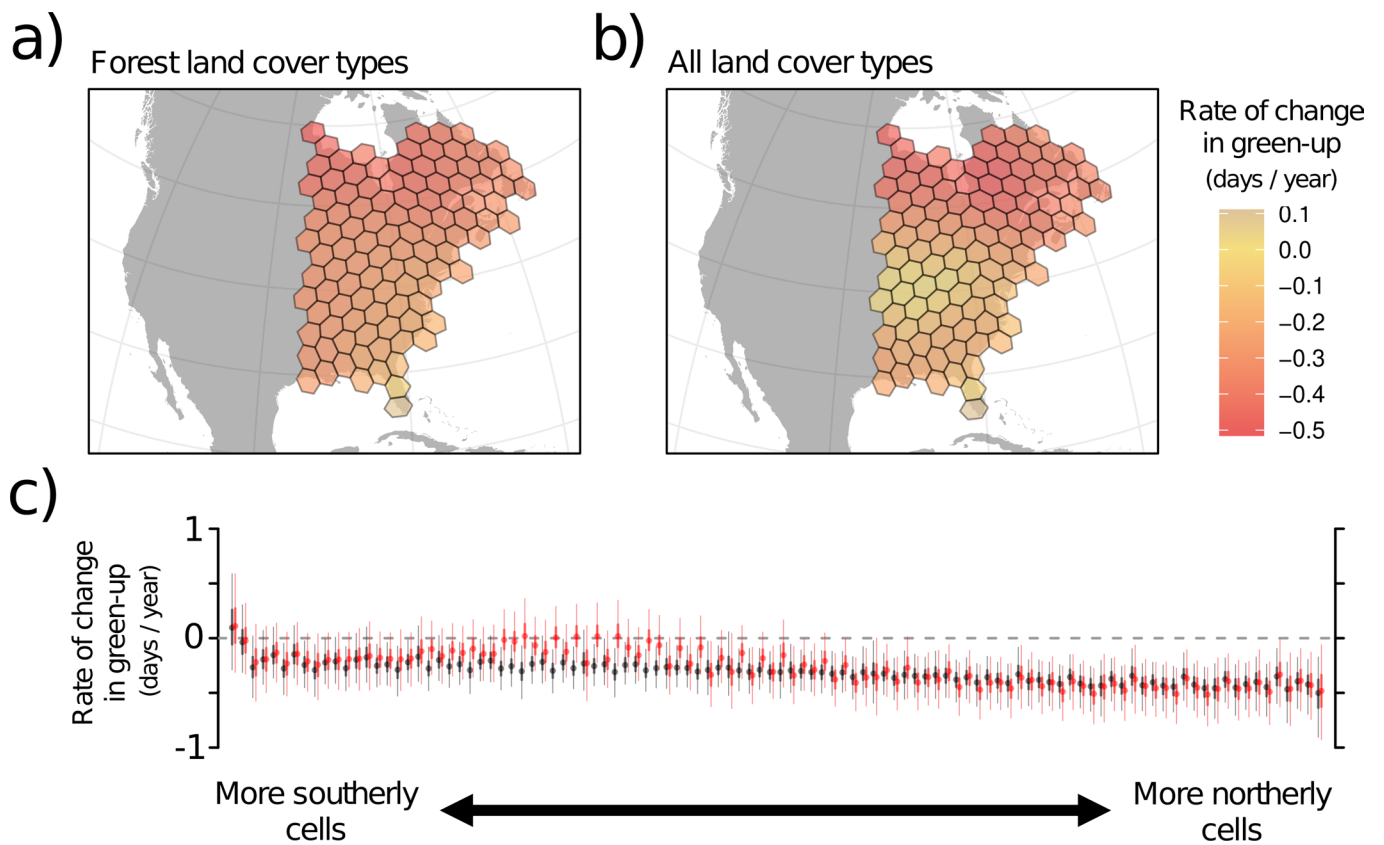
**Extended Data Fig. 3 | Data processing pipeline using red-eyed vireo (*Vireo olivaceus*) as an example.** Estimates of arrival (half-maximum) were derived from generalized additive models (GAMs), which were then used as input for the intrinsic autoregressive (IAR) model to produce spatially smoothed estimates of arrival. The plot at the far left shows GAM results for a single cell-year for this species. Circles at the top of the plot represent eBird checklists in which red-eyed vireo was recorded, while circles at the bottom of the plot represent eBird checklists in which red-eyed vireo was not recorded. The black line represents the mean GAM fit, while the dashed red lines represent the 95% credible intervals. The solid blue and dashed blue lines represent the mean estimate and 95% credible intervals for the half-maximum, respectively. The plots in the centre column of the figure represent the estimated arrival date of this species over the study area for 2006. The plot at top centre represents the GAM-derived arrival estimates, while the plot at bottom centre represents the IAR-derived arrival estimates. Blue hues represent later arrival dates while pink hues represent earlier arrival dates for a given cell. The plots at far right represent a subset (the region bounded by the black box) of the maps in the centre column of the figure. Numbers in black represent the posterior mean of the arrival day (ordinal date), while the white numbers represent the posterior standard deviation of the arrival day.



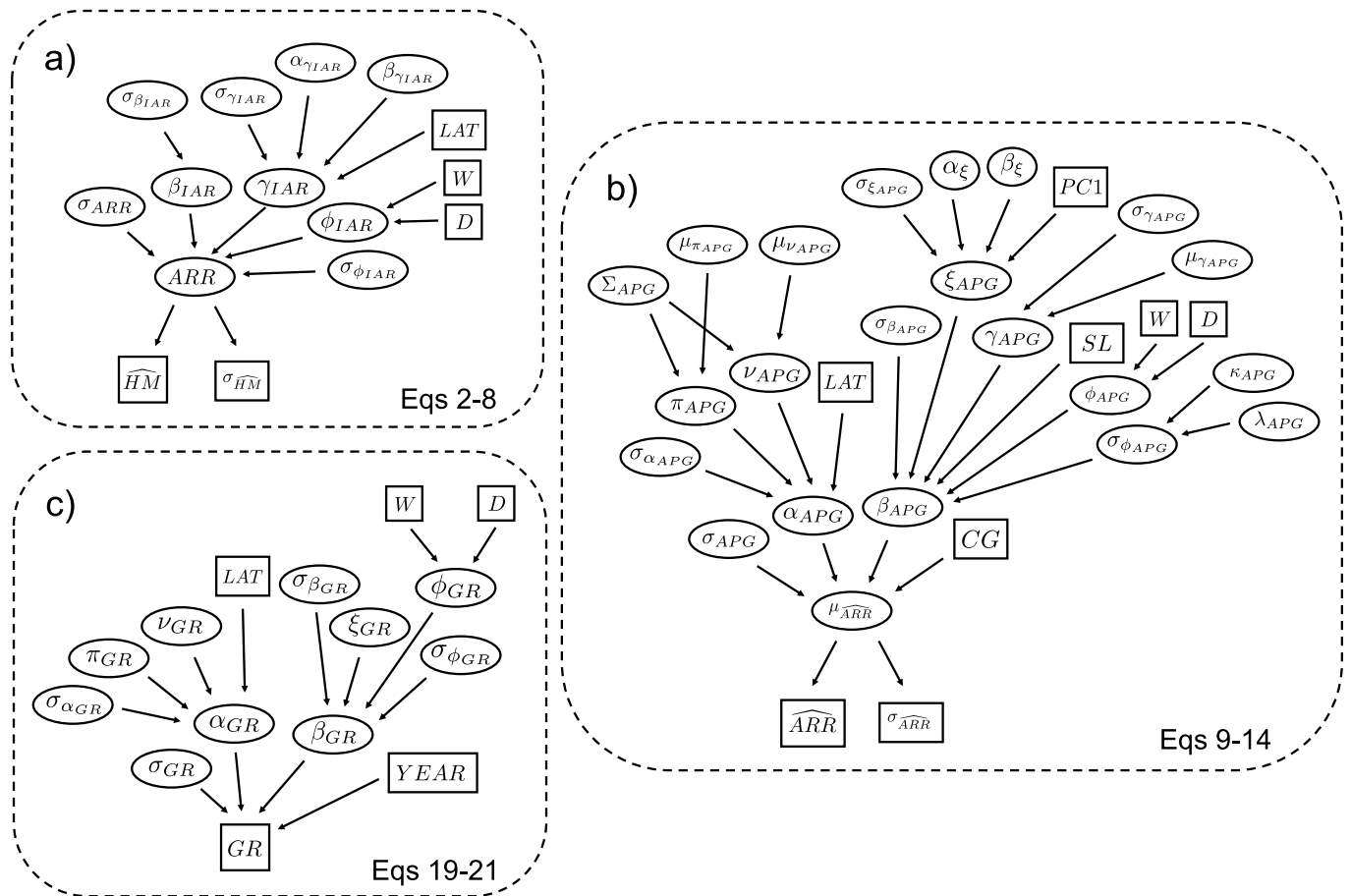
**Extended Data Fig. 4 | Number of cells across the study area that met data requirements for each species and year.** Red hues represent more cells while white hues represent fewer cells. Only species that met minimum data requirements are shown. Since species-years with fewer than 3 valid cells were not run as a part of the IAR model (see Methods), each species-year has either 0 or 3 or greater valid cells.



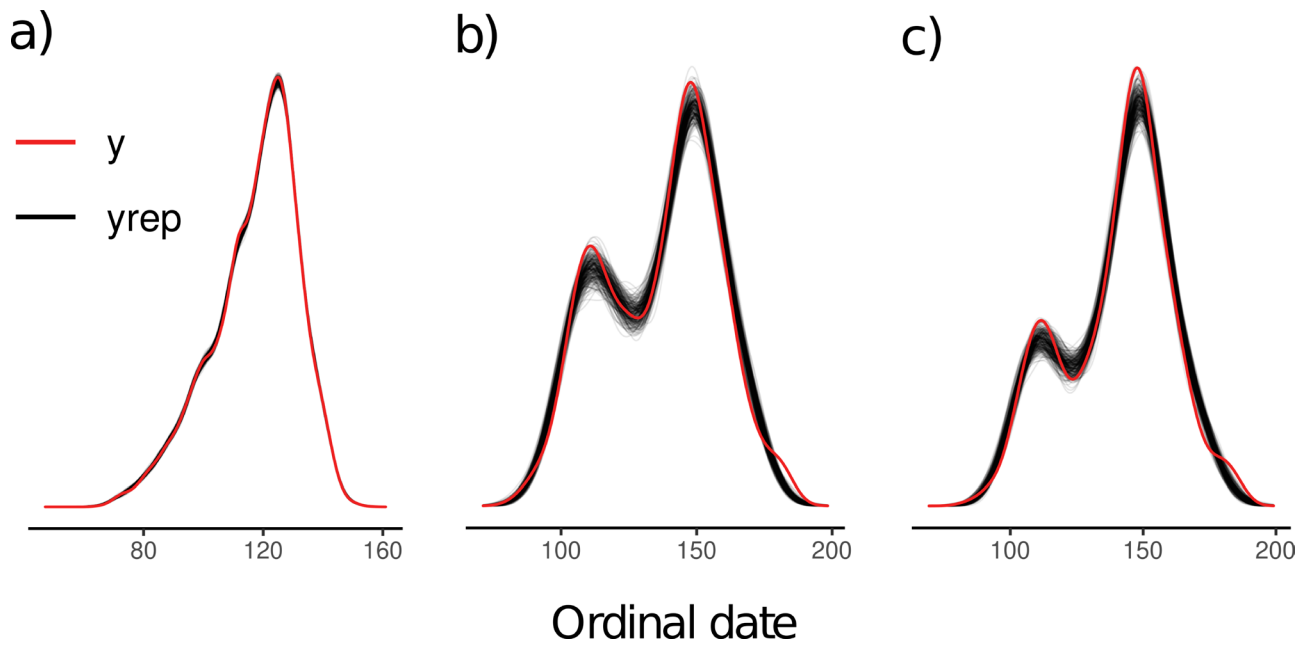
**Extended Data Fig. 5 |** Posterior estimates for a)  $\xi_{APG}$  (the species-specific phenological sensitivities; equation 11) and b)  $\gamma_{APG}$  (the species-specific effect of latitude on phenological sensitivities; equation 11). Points represent posterior medians, thick lines represent 50% credible intervals, thin lines represent 95% credible intervals. The dashed grey line represents zero in each case.



**Extended Data Fig. 6 | Rate of change in green-up from 2002–2017 over the study area for (a) forest land cover types, and (b) all land cover types.** Colours for (a) and (b) represent the cell-specific posterior mean estimates of the rate of change in green-up over time (days change per year) with red hues representing more negative trends over time (earlier green-up) and yellow hues representing no trend over time. **c.** Posterior estimates for cell-specific rate of change in green-up for forest land cover types (black) and all land cover types (red). Points represent the posterior median estimates for the rate of change of each cell (ordered by latitude), thick lines represent 50% credible intervals, thin lines represent 95% credible intervals. The dashed grey line represents zero.



**Extended Data Fig. 7 | Directed acyclic graphs (DAGs) outlining the hierarchical models used in this study.** Boxes represent variables that were provided to the model, while ovals represent parameters estimated by the model. Corresponding equation numbers for each DAG given in lower right of each bounded box. Lettering corresponds to that shown in Supplementary Table 2, which provides descriptions of each variable represented in the DAGs.



**Extended Data Fig. 8 | Density plots for observed response variable data ( $y$ ; corresponding to IAR-derived arrival dates for (a) and green-up dates for (b) and (c)) and response variable data simulated from the posterior predictive distribution ( $y_{rep}$ ).** These plots were used for graphical posterior predictive checks, to ensure that data simulated from the model were similar to the observed data for models examining (a) the sensitivity of bird arrival to vegetation phenology (Eqs. 9-14), (b) trends in green-up over time for forest land cover types (Eqs. 19-21), and (c) trends in green-up over time for all land cover types (Eqs. 19-21). Curves in red are a representation of the density of all response data used to fit each model. Curves in black are a representation of the density of data simulated from the posterior predictive distribution. Each iteration of the posterior chain yields a simulated dataset. Here 250 datasets simulated from the posterior predictive distribution are displayed (250 separate black lines). The general similarities between the red lines and black lines demonstrate that the models simulate data similar to the observed data.